7th International Symposium on Hydraulic Structures Aachen, Germany, 15-18 May 2018
ISBN 978-0-692-13277-7 DOI: 10.15142/T3FS9Q

Air Bubble Entrainment in Breaking Bores: Physical and Numerical CFD Modelling

X. Leng[1], H. Chanson[1] & P. Lubin[2]
[1]*The University of Queensland, School of Civil Engineering, Brisbane QLD, Australia*
[2]*Université de Bordeaux, Bordeaux-INP, I2M, Pessac, France*
E-mail: h.chanson@uq.edu.au

Abstract: *A positive surge or bore is an unsteady rapidly-varied open channel flow characterised by a rise in water surface elevation. After formation, the bore is traditionally analysed as a hydraulic jump in translation and its leading edge is characterised by a breaking roller for Fr_1 > 1.3–1.5. The roller is a key flow feature characterised by intense turbulence and air bubble entrainment. Herein detailed air-water flow measurements were conducted in breaking bores propagating in a large-size channel. The data showed a relatively steep roller, with a short and dynamic bubbly flow region. The results were used to validate a Computational Fluid Dynamics (CFD) model of breaking bores. The instantaneous void fraction and bubble distribution data showed systematically a lesser aeration region in the physical model, compared to the numerical data. The differences may be linked to some limitation of the CFD modelling.*

Keywords: *Breaking bores, air bubble entrainment, computational fluid dynamics, CFD modelling, physical modelling, two-phase flow, unsteady flow motion.*

1. Introduction

In an estuary, a tidal bore is a hydraulic jump in translation generated at the leading edge of the tide during the early flood tide under spring macro-tidal conditions in a narrow funnelled channel (Chanson 2011a). A related physical process is the positive surge in an open channel (Tricker 1965). Hydraulic engineering applications encompass positive surges in open channels, also called compression wave or hydraulic jump in translation. Examples include rejection surges and load acceptance surges in hydropower canals, and positive surges in water supply channels following gate operation (Henderson 1966, Montes 1998). After formation, the bore may be analysed as a hydraulic jump in translation, in the system of reference in translation with the surge. Its leading edge is characterised by a breaking roller for Fr_1 > 1.3–1.5, where Fr_1 is the surge Froude number (Favre 1935, Leng and Chanson 2017).

A key feature of breaking bores is the roller, a highly turbulent region characterised by large-scale vortices, and air bubbles and air packets entrapped at the impingement of the inflow into the roller (Fig. 1). Figure 1 (Left) presents the roller of the Qiantang River bore: on the photograph, the roller was almost 4.5-5 m high, near 2.8 km wide and the surge Froude number was about 2. When air bubble entrainment occurs at breaking wave impact, the entrapped air can be compressed and result in massive pressure shock wave (Peregrine 2003, Bredmose et al. 2009). While the impact of breaking surge on hydraulic structures was documented (Lu et al. 2009), the effect of aeration cannot be modelled in absence of relevant detailed validation data sets. The studies of air entrainment in breaking bores remain restricted to the preliminary work of Leng and Chanson (2015) and a few limited analogies to stationary hydraulic jumps (Wang et al. 2017).

In this study, both physical and Computational Fluid Dynamics (CFD) investigations were conducted with a focus on the air-water flow properties in a breaking bore roller. Detailed laboratory experiments were conducted in a large size facility, with a combination of ultra-high-speed video observation as well as unsteady phase-detection measurements in the bore roller. CFD numerical modelling was based upon the incompressible Navier-Stokes equations in its two-phase flow forms using Large Eddy Simulation (LES). It is the aim of this contribution to develop the first detailed investigation of air-water flow characteristics of breaking bores and surges.

2. Breaking Bore Modelling

2.1. Physical Model

The experimental facility was a large rectangular channel, with a 19 m long and 0.7 m wide test section set with a channel slope S_o = 0.0075. The test section was made of glass side walls and smooth PVC bed. The breaking bore was generated by the fast closure of a Tainter gate located next to the downstream end of the channel at x = 18.1 m, where x is measured from the upstream end of the channel, and the bore propagated upstream.

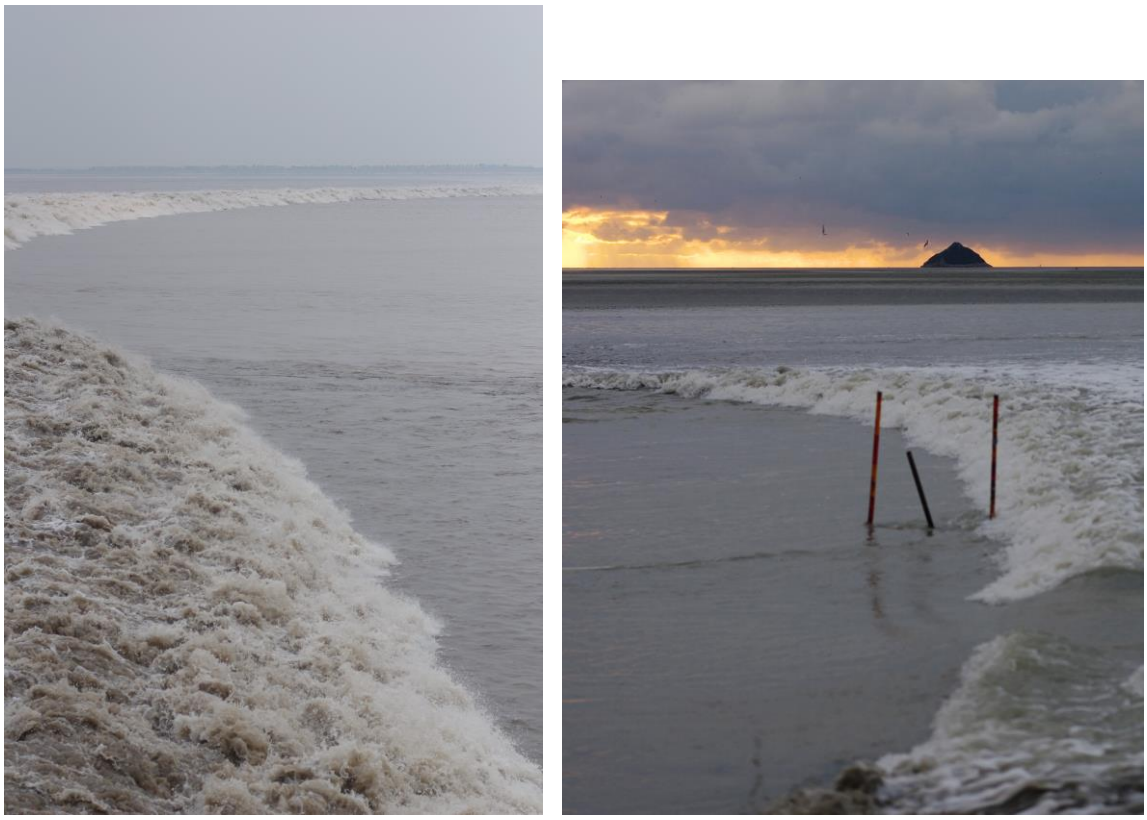

Figure 1. Breaking tidal bores - Left: Breaking bore of the Qiantang River, near Yanguan (China) on 11 October 2014, with bore propagation from left to right; Right: Breaking bore of the Sélune River at Pointe du Grouin du Sud (France) on 24 September 2010, with bore propagation from right to left

The discharge was measured by a magneto flow meter. In steady flows, the water depths were measured using pointer gauges. The unsteady water depths were recorded with acoustic displacement meters (ADMs), spaced along and above the channel between x = 18.17 m, 17.41 m, 9.96 m, 8.50 m, 6.96 m. All acoustic displacement meters (ADMs) were calibrated against point gauge measurements in steady flows and sampled at 200 Hz.

The air-water flow properties were recorded using an array of three dual-tip phase-detection probes located at x = 8.50 m (Fig. 2). One probe located about the channel centreline was used as a reference, following Chanson (2004). Its position (z = 0.105 m) remained unchanged for the entire duration of the experiments. The time origin (t = 0) was selected when the leading sensor of the reference phase-detection probe first detected an air-to-water interface, for all experimental runs. The other two probes were placed at a same vertical elevation, different from the reference probe, and their leading sensor was at the same longitudinal position as the leading sensor of the reference probe. Each dual-tip probe was equipped with two needle sensors developed at the University of Queensland. Each needle sensor consisted of a silver wire (Ø = 0.25 mm) insulated from the outer needle. All sensors were aligned with the longitudinal direction, facing downstream and designed to pierce the bubble interfaces in the bore roller. The probe sensors were excited simultaneously by an electronic system (Ref. UQ82.518) designed with a response time less than 10 μs. The sampling rate was 100 kHz per sensor for all probes.

The experiments were performed with a breaking bore (Fr_1 = 2.2). Two series of experiments were conducted. During each series, the reference probe was always set at the same longitudinal, transverse and vertical location (x = 8.50 m, y = 0.324 m. z = 0.105 m) and it was used as time reference. In experiment series 1 and 2, the other two dual-tip phase detection probes were positioned close to the channel centreline. In series 1, the experiments were repeated for different probe tip elevations: at each elevation z, one run was performed. During experiment series 2, the measurements were repeated 5 times at several vertical elevations: 0.105 m < z < 0.205 m.

The voltage outputs of the phase-detection conductivity probes were processed using a single threshold technique to convert the instantaneous voltage signals into instantaneous void fraction and to calculate bubble interfacial times. The single threshold technique is a very robust method in free-surface flows, and the threshold was herein set at 50% of the air-water voltage range to cover the wide range of void fractions in the whole air–water flow column following Toombes (2002), Chanson (2002,2016a), and Felder and Chanson (2015). The

probe signal output is the instantaneous void fraction c, with c = 1 in air and c = 0 in water. Further details on the signal processing are discussed in Leng and Chanson (2018).

Figure 2. High-speed photograph (shutter speed: 1/2,000 s) of probe array immediately before roller impact, with bore direction from top right to bottom left, during the physical experiments—The reference probe is on the far left

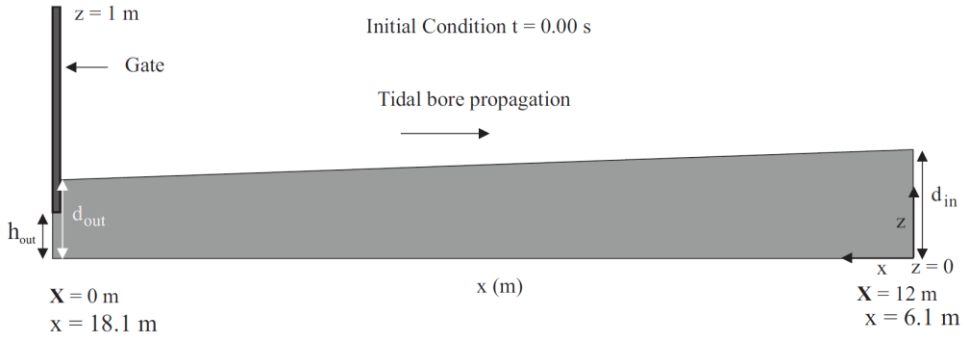

Figure 3. Definition sketch of the numerical domain and physical domain; **X** is the distance from the left boundary (i.e. gate); x is the distance from the upstream end of the physical channel.

2.2. Numerical Model

The numerical model was the Computational Fluid Dynamics (CFD) code Thétis developed by I2M laboratory of the University of Bordeaux (France). The model solved the Navier-Stokes equations in its incompressible two-phase flow form between non-miscible fluids. The two fluids were air and water. A phase function α (α = 1-c), called the color function or liquid fraction, is used to locate the different fluids with α = 0 in air and α = 1 in water. The governing equations are basically the Large Eddy Simulation (LES) of an incompressible fluid flow classically derived by applying a convolution filter to the unsteady Navier-Stokes equations (Lubin et al. 2010, Leng et al. 2017).

The space derivatives of the inertial term are discretised by a hybrid upwind-centered scheme and the viscous terms is approximated by a second-order centered scheme (Lubin et al. 2006). The interface tracking is done using a Volume of Fluid (VOF) method with a Piecewise Linear Interface Calculation (PLIC). This method has the advantage of building a sharp interface between air and water. The time discretization is implicit and the equations are discretised on a staggered grid thanks to a finite volume method. The MPI library HYPRE is used to solve the linear system of the prediction and correction steps (Falgout et al. 2006). The time steps are dynamically calculated to insure a CFL condition inferior to 0.2. The numerical model has been proved accurate through a variety of coastal applications and numerous test cases (Lubin 2004; Lubin et al. 2006). Earlier CFD studies of tidal bores by Simon et al. (2011) and Khezri (2014) were also based upon this model.

Breaking bores with Froude numbers Fr_1 = 2.1 were simulated using a two-dimensional (2D) model. The numerical domain was 12 m in the longitudinal (stream wise) direction and 1 m in the vertical direction (Fig. 3). A no-slip condition was imposed at the lower boundary (z = 0 m) and a Neumann condition was used at the upper boundary (z = 1 m). At the end of the domain (x = 12 m), a wall boundary was imposed to act like a closed gate to reproduce the experimental generation process. The bed slope was set at S_o = 0.0075 as the experimental

channel. To generate a breaking bore of $Fr_1 = 2.1$, the numerical gate was fully closed with no gap underneath i.e. $h_{out} = 0$. The initial conditions of the 2D models consisted of a water trapezoid, with higher depth at the inlet (d_{in}) and lower depth at the outlet (d_{out}) to approximate the gradually-varied flow in the physical channel. All initial and boundary parameters were preset using experimental results of the same flow condition. The 2D numerical models were started at the gate closure, i.e. initial condition t = 0 at gate closure with the immediate generation of a bore. The simulation was stopped after the bore reached the inlet of the numerical domain, which was considered one single run. Due to limitation in computational time and capacity, each flow condition was only simulated for one run by the numerical CFD model. For the same initial conditions as the physical experiment and for the same boundary conditions, the numerical model yielded a breaking bore, with the following characteristics at x = 8.5 m (X = 9.6 m): $Fr_1 = 2.07$, U = 0.84 m/s.

The grid size of the 2D model was 1 cm squares uniform mesh, based upon initial tests. Preliminary tests were conducted with three mesh grid densities for the above flow conditions, the smallest mesh being 0.5 cm squares. No convergence was observed when the mesh grid was refined for this flow condition. Rather, the numerical model became more unstable as the grid became finer. Despite being the coarsest one, the selected mesh grid density, i.e. 1 cm square uniform, gave the best comparison to physical results.

3. Breaking Bore Roller Characteristics

3.1. Presentation

The breaking bore was characterised by its marked roller, with spray and splashing ahead and above the roller, air bubble entrainment at the roller toe and through the roller's upper free-surface, and rapid fluctuations in space and time of the roller shape. Figure 4 shows typical instantaneous views of the bore roller and air-water structures. In front of the roller, the free-surface was flat. No upward free-surface curvature was recorded ahead of the roller, as previously reported for $Fr_1 > 2$ (Leng and Chanson 2015). With the arrival of the roller toe, the flow became strongly turbulent with large vertical fluctuations and a two-phase bubbly structure. High amplitude motions and strong fluctuations in time and space were evidenced by high-shutter speed photography, high-speed movies and acoustic displacement meter data in the roller region.

Observations showed the presence of water filaments and droplets ejected in front of the roller. Similar observations of droplet ejections were seen in the breaking bore of the Qiantang River (China) by the authors on 23 September 2016 in Yanguan. In the Qiantang River bore, droplets could be ejected up to 1 m to 1.5 m ahead of the roller toe.

The roller front consisted of foamy mixtures and complicated air-water flow structures. Air-water flow structures constantly evolved in shape and size, in response to the turbulent fluctuations and interactions with the roller and free-surface. Detailed photographs showed large air-water structures, ejected upwards in all directions (upstream, downstream, upwards, sideway), and re-attaching the roller, either by gravity, re-attachment to another structure or by being caught up by some overturning motion (Fig. 4). The air-water flow structures tended to be similar to gas-liquid structures observed in breaking hydraulic jumps (Chanson 2011b, Chachereau and Chanson 2011) and in the upper region of high-speed self-aerated flows (Cain and Wood 1981, Chanson 1997a).

Below the free-surface, a large number of bubbles were entrained within the roller. Both individual bubbles and bubble groups were observed. Visual observations showed rapidly evolving bubble shapes and numbers in response to turbulent shear, bubble-bubble interactions and bubble-free-surface interactions (Fig. 4). At the rear of the roller, large aerated vortex filaments, and bathtub-like or tornado-like vortices were seen underwater. These filaments were similar to those occurring under plunging breaking waves (Lubin and Glockner 2015) and in turbulent shear flows (Hunt et al. 1988). For completeness, long aerated vortex filaments were also observed during the rapid gate closure herein. The gate closure induced some water pile-up against the gate and overturning, in a manner similar to a plunging breaking waves, before the bore roller detached from the gate and propagated upstream as detailed by Sun et al. (2016). Herein the filament lengths ranged typically from about 10 mm to over 50 mm, with millimetric bubbles between 1 mm and 5 mm sizes. While the underwater filament were observed at the rear of the roller, where the void fraction was very low, their extremities were often not distinguishable because of the chaotic motion of the highly aerated flow, and could be obscured by bubble clouds and air-water structures. In the present study, however, it was not clear what the mechanisms responsible for the filament generation and evolution were.

3.2. Liquid Fraction Distributions

During experiments series 1 and for each run, the reference probe was set at the same longitudinal, transverse and vertical location and its detection of the first air-to-water interface was used as time reference. The

experiments were repeated at 33 different elevations: that is, one run was performed at each elevation z. Typical instantaneous liquid fraction (1-c) data in the bore roller are shown Figure 5a. Figure 5 presents two-dimensional distributions of liquid fraction. Figure 5a shows instantaneous physical data, while numerical data are presented in Figure 5b. Note the different scales between Figures 5a and 5b. The physical data indicated a shorter and thinner air-water flow region than the numerical prediction. This might be linked to the mesh grid size and density of the model. In practice, to simulate a small inclusion (bubble or droplet), five to ten mesh grid points per diameter are required (e.g. Li et al. 2010, Wang et al. 2016). With the present mesh grid size (10 mm squares in each direction), the smallest physically-meaningful bubble would have a 50 mm dimension. Further, the transverse dimension was not included in a 2D model, resulting in the momentum transport in that direction being completely ignored. The energy dissipation due to the turbulent breaking roller was not accounted for in the 2D model, which could also lead to an over-energetic and overly long air-bubbly region.

(a)

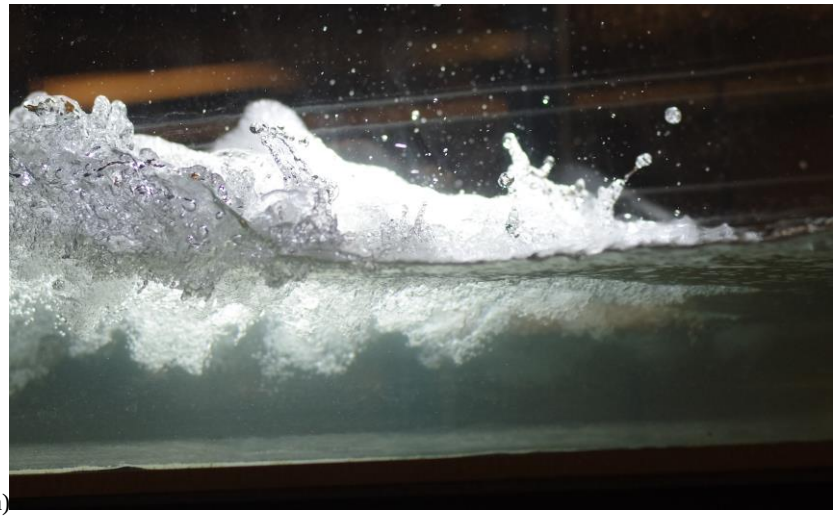

(b)

(c)

Figure 4. High-speed photographs of breaking bore roller (Fr_1 = 2.18, d_1 = 0.097 m, U = 0.64 m/s) - (a) Roller toe leading edge, propagating from left to right (shutter speed 2,000 s); (b) Overturning at the toller leading edge (shutter speed 1/2,000 s); (c) air-water bubbly structure in front of phase-detection probe array (shutter speed 1/8,000 s)

Overall the data showed that the air-water flow region of the roller was relatively small (Fig. 5). The finding was consistent with air-water flow measurements in stationary hydraulic jumps at low Froude numbers (Chachereau and Chanson 2011). A characteristic feature of breaking bore roller was the large amount of spray and droplets above and in front of the roller. The spray region interacted with the atmosphere and induced some short-lived air flux above the water surface. A related effect of air bubble entrainment was the relatively loud noises generated by the bore roller. The sound of the breaking bore was relatively low-pitch and had a characteristic frequency close to the collective oscillations of bubble clouds, linked to a transverse dimension of the bore roller (Chanson 2016b).

4. Roller Longitudinal Profile

The instantaneous vertical distributions of liquid fraction (1-c) were analysed in terms of the instantaneous clear-water depth d defined as:

$$d = \int_{z=0}^{+\infty} (1 - c(z,t)) \times dz \quad (1)$$

where z is the vertical elevation and t is the time, with t = 0 corresponding to the detection of the first air-to-water interface by the leading sensor of the reference probe. The instantaneous clear-water depth d is comparable to the equivalent clear-water depth commonly used in high-velocity free-surface steady flows (Wood 1984,1985, Chanson 1997b), albeit the latter is calculated in terms of a time-averaged void fraction C. In Figure 5a, the experimental results are compared with the acoustic displacement meter (ADM) data, namely the 25%, 50% and 75% percentiles of the ensemble, denoted d_{25}, d_{50}, and d_{75} respectively. A detailed comparison between the characteristic depth data derived from air-water flow measurements and the acoustic displacement meter (ADM) data indicated that the instantaneous clear-water depth d was about the median ADM depth data (Fig. 6a). Although the results were obtained in a rapidly-varied unsteady flow, the finding was close to observations in stationary hydraulic jumps (Chachereau and Chanson 2011, Wang et al. 2015) and in skimming flows on stepped spillway (Felder and Chanson 2014).

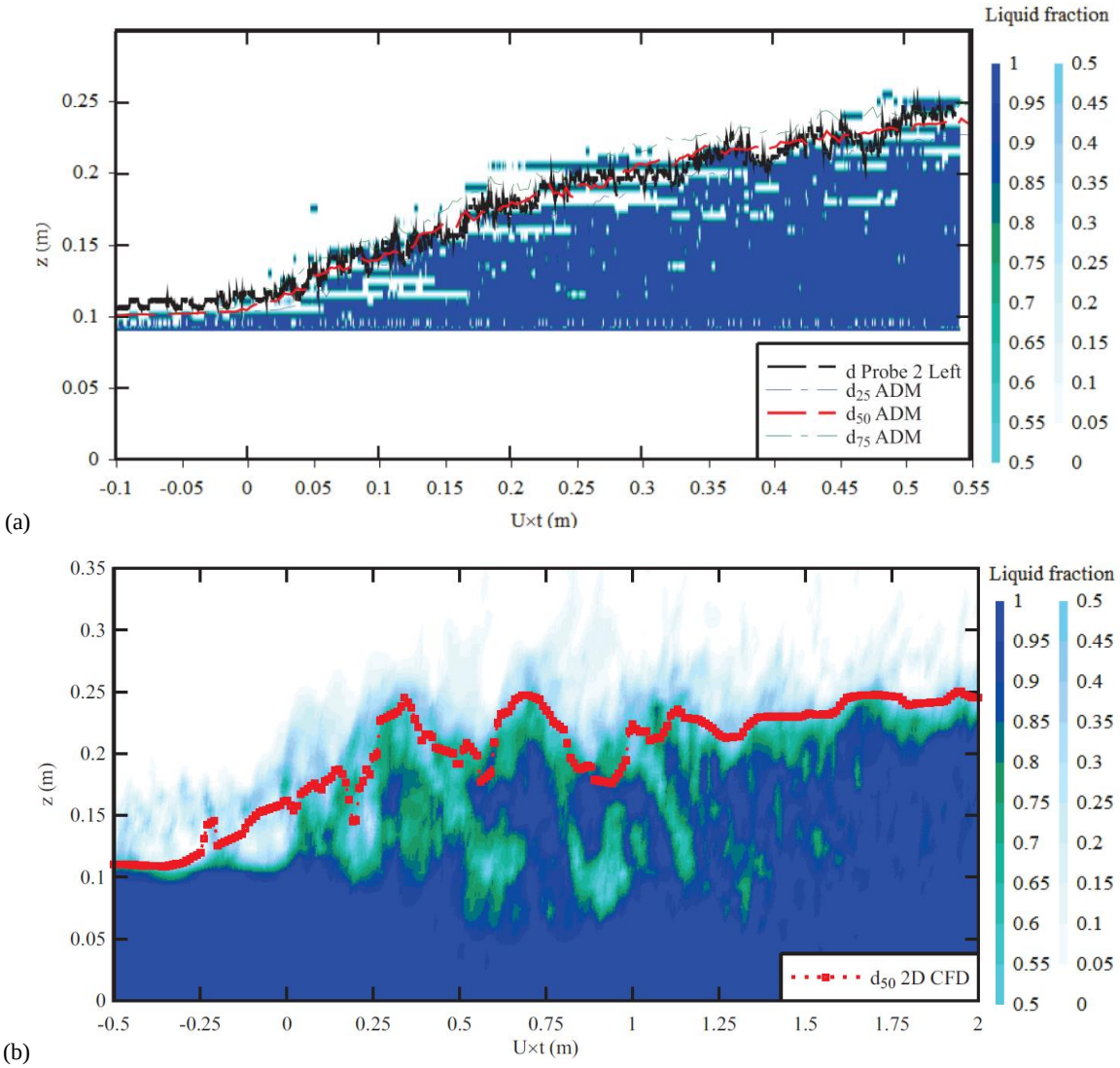

Figure 5. Contour plot of liquid fraction in a breaking bore and comparison with characteristic depth data - (a) Physical data: instantaneous liquid fraction, Probe 2, right sensor: x = 8.50 m, y = 0.231 m, Flow conditions: Fr_1 = 2.18, d_1 = 0.097 m, U = 0.64 m/s; comparison with clear-water depth (Eq. (1)) and acoustic displacement meter data (25%, 50%, 75% percentiles, coloured lines) (b) 2D CFD data: ensemble-averaged over 10 time steps; x ~ 8.5 m, Flow conditions: Fr_1 = 2.07, d_1 = 0.110 m, U = 0.84 m/s; comparison with 50% colour function depth

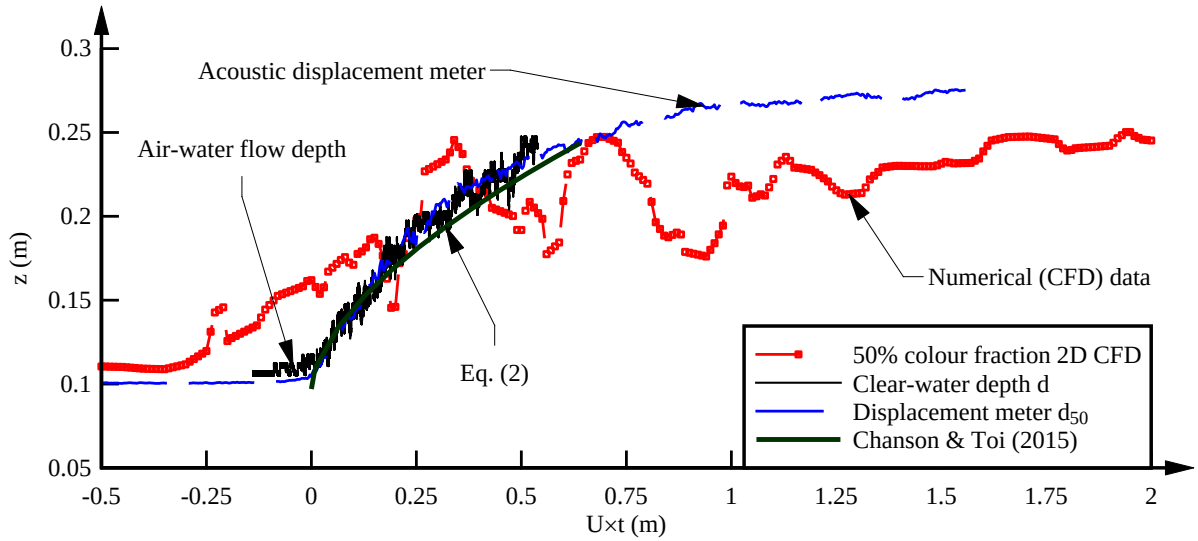

(a) Characteristic depth: clear-water depth d, median acoustic displacement meter data, 50% colour function depth – Comparison with Equation (2) (Chanson and Toi 2015)

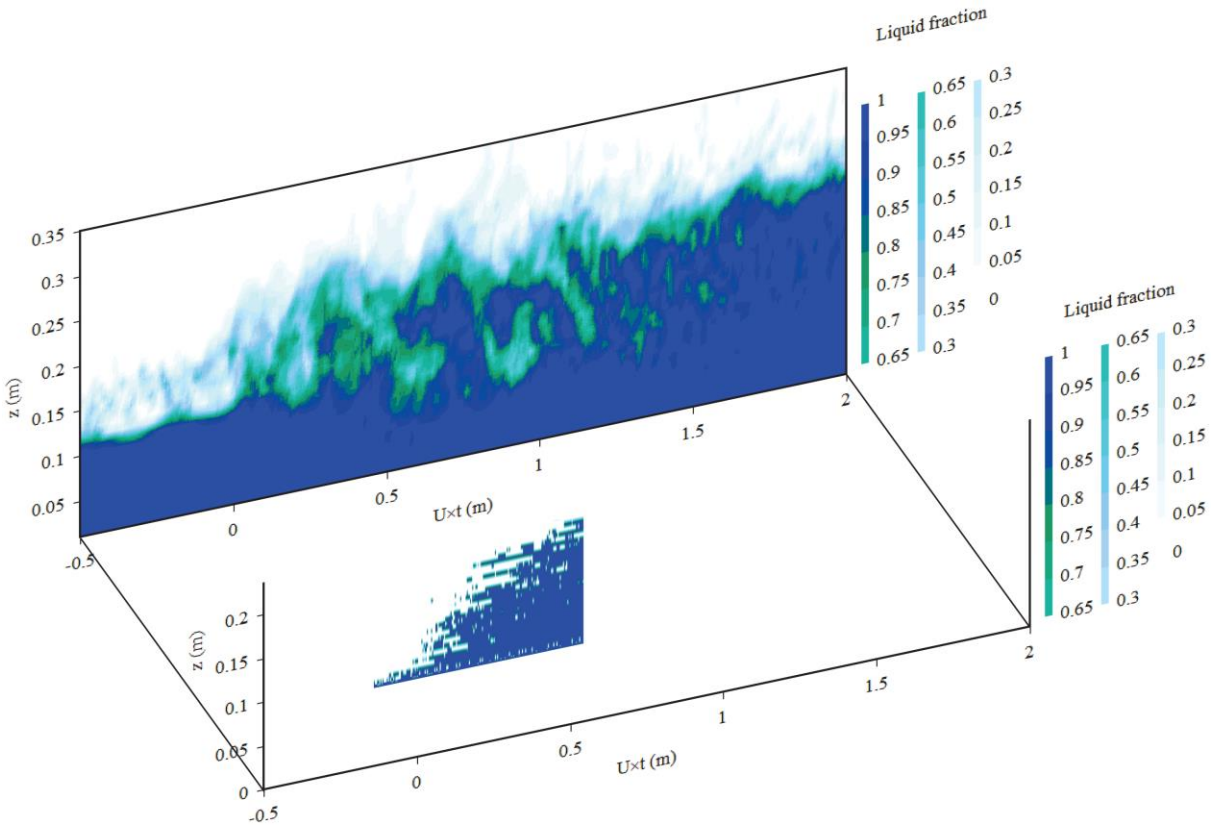

(b) Liquid fraction in the breaking bore roller - Both contour plots have same axis range, with laboratory data in foreground and CFD numerical data in background – Bore propagation from right to left

Figure 6. Breaking bore profile: comparison between physical laboratory data and CFD numerical data – Tidal bore flow conditions: Fr_1 = 2.18, d_1 = 0.097 m, U = 0.64 m/s (Physical model); Fr_1 = 2.07, d_1 = 0.110 m, U = 0.84 m/s (Numerical CFD model)

The physical data showed some longitudinal profile of the bore roller that was very close to past tidal bore observations (Chanson and Toi 2015), classical results in hydraulic jumps (Chanson 2011b, Wang 2014) and theoretical considerations (Valiani 1997). That is, the free-surface profile presented the same self-similar profile first proposed by Chanson and Toi (2015) based upon field and laboratory breaking tidal bore observations:

$$\frac{d - d_1}{d_2 - d_1} = \left(\frac{x - x_1}{L_r} \right)^{0.6} \quad (2)$$

where d_2 is the conjugate depth, x_1 is the roller toe co-ordinate and L_r is the roller length. Present physical data matched very closely Equation (2), as seen Figure 6a. In Figure 6a, the 50% colour function location is also shown for completeness.

In comparing the physical and numerical air-water flow data (Fig. 5 and 6b), the 2D CFD simulation results agreed well with the experimental data qualitatively. But the numerical model was unable to reproduce the bore roller front with the same steepness as observed in the experimental model. In Figure 6b, the physical and numerical data are presented with the same horizontal and vertical axis scales to emphasise the quantitative comparison. The steepness of the bore front in the numerical simulation was much flatter as illustrated in Figure 6. The numerical data showed further a greater aeration of the roller, as well as a lesser de-aeration in the wake of the bore front compared to the physical observations (Fig. 6b). In Figure 6b, the flow aeration behind the roller was negligible in laboratory and no void fraction data was reported in the physical model (Fig. 6b, foreground results).

5. Conclusion and Recommendations

Positive surges are highly-unsteady extremely-turbulent open channel flows. Applications range from tidal bores in estuaries to load acceptance surges in tailwater canals, rejection surges in hydropower canals, and positive surges in irrigation canals following rapid control gate operation. Herein detailed unsteady air-water flow measurements were conducted in breaking bores propagating in a large-size channel. The physical results were used to validate a Computational Fluid Dynamics (CFD) model of breaking bores. The numerical modelling was based upon the solution of the incompressible two-dimensional (2D) Navier-Stokes equations in its two-phase flow forms using Large Eddy Simulation (LES). The physical experiments were performed in a 19 m long 0.7 m wide prismatic rectangular channel. The two phase flow measurements were conducted using an array of three dual-tip phase detection probes and experiments were repeated to perform ensemble-averaging. The physical data showed a relatively steep roller front, with a short and dynamic air-water bubbly flow region.

Systematic comparisons between numerically simulated free-surface evolution and experimental observations were conducted. Overall, the free-surface variations simulated by the CFD model agreed qualitatively with the experimental data. The two-phase flow properties indicated marked quantitative differences between the CFD results and the physical results. The instantaneous void fraction and bubble population physical data showed systematically a lesser aeration region, compared to the numerical data. The differences may be linked to some limitation of the CFD modelling.

This study showed further why a detailed validation process is crucial, involving a sound physical knowledge of the flow. A comparison of numerical model results and experimental data is mandatory, over broad ranges of flow properties. In the case of breaking bores, a complete characterisation of the air-water flow processes necessitates to repeat the physical experiments and to perform ensemble-averaging. Great care is absolutely necessary to ensure the repeatability of the experiments and the synchronisation between repeated experiments, as first shown in tidal bore flows by Chanson and Docherty (2012) and Leng and Chanson (2016). Without such high-quality physical data, any CFD validation would be meaningless and lack credibility. Simply "*no [high-quality] experimental data means no validation*" (Roache 2009).

6. Acknowledgements

The authors acknowledge the helpful assistance of Dr Hang Wang (The University of Queensland, Australia) and Dr. Stéphane Glockner (Université de Bordeaux, I2M, Laboratoire TREFLE, Pessac, France). They acknowledge the technical assistance of Jason Van Der Gevel and Stewart Matthews (The University of Queensland). The authors also wish to thank the Aquitaine Regional Council for financial support towards a 432-processor cluster investment, located in the I2M laboratory. This work was granted access to the HPC resources of CINES, under allocation 2016-x2012026104 made by GENCI (Grand Equipement National de Calcul Intensif). Computer time for this study was also provided by the computing facilities at MCIA (Mésocentre de Calcul Intensif Aquitain) of the Université de Bordeaux and of the Université de Pau et des Pays de l'Adour.

7. References

Bredmose, H., Peregrine, D.H., and Bullock, G.N. (2009). "Violent breaking wave impacts. Part 2: modelling the effect of air." *Journal of Fluid Mechanics*, Vol. 641, pp. 389-430 (DOI: 10.1017/S0022112009991571).

Cain, P., and Wood, I.R. (1981). "Measurements of Self-aerated Flow on a Spillway." *Journal of Hydraulic Division*, ASCE, 107, HY11, pp. 1425-1444.

Chachereau, Y., and Chanson, H. (2011). "Bubbly Flow Measurements in Hydraulic Jumps with Small Inflow Froude Numbers." *International Journal of Multiphase Flow*, Vol. 37, No. 6, pp. 555-564 (DOI: 10.1016/j.ijmultiphaseflow.2011.03.012).

Chanson, H. (1997a). "Air Bubble Entrainment in Open Channels. Flow Structure and Bubble Size Distributions." *International Journal of Multiphase Flow*, Vol. 23, No. 1, pp. 193-203 (DOI: 10.1016/S0301-9322(96)00063-8).

Chanson, H. (1997b). "Air Bubble Entrainment in Free-Surface Turbulent Shear Flows." *Academic Press*, London, UK, 401 pages (ISBN 0-12-168110-6).

Chanson, H. (2002). "Air-Water Flow Measurements with Intrusive Phase-Detection Probes. Can we Improve their Interpretation?" *Journal of Hydraulic Engineering*, ASCE, Vol. 128, No. 3, pp. 252-255 (DOI: 10.1061/(ASCE)0733-9429(2002)128:3(252)).

Chanson, H. (2004). "Unsteady Air-Water Flow Measurements in Sudden Open Channel Flows." Experiments in Fluids, Vol. 37, No. 6, pp. 899-909 (DOI: 10.1007/s00348-004-0882-3).

Chanson, H. (2011a). "Tidal Bores, Aegir, Eagre, Mascaret, Pororoca: Theory and Observations." *World Scientific*, Singapore, 220 pages (ISBN 9789814335416).

Chanson, H. (2011b). "Hydraulic Jumps: Turbulence and Air Bubble Entrainment." *Journal La Houille Blanche*, No. 1, pp. 5-16 & Front cover (DOI: 10.1051/lhb/2011026).

Chanson, H. (2016a). "Phase-Detection Measurements in Free-Surface Turbulent Shear Flows." *Journal of Geophysics and Engineering*, Vol. 13, No. 2, pp. S74-S87 (DOI: 10.1088/1742-2132/13/2/S74).

Chanson, H. (2016b). "Atmospheric Noise of a Breaking Tidal Bore." *Journal of the Acoustical Society of America*, Vol. 139, No. 1, pp. 12-20 (DOI: 10.1121/1.4939113).

Chanson, H., and Docherty, N.J. (2012). "Turbulent Velocity Measurements in Open Channel Bores." European Journal of Mechanics B/Fluids, Vol. 32, pp. 52-58 (DOI 10.1016/j.euromechflu.2011.10.001) (ISSN 0997-7546).

Chanson, H., and Toi, Y.H. (2015). "Physical Modelling of Breaking Tidal Bores: Comparison with Prototype Data." *Journal of Hydraulic Research*, IAHR, Vol. 53, No. 2, pp. 264-273 (DOI: 10.1080/00221686.2014.989458).

Falgout, R., Jones, J. and Yang, U. (2006). "The design and implementation of hypre, a library of parallel high performance preconditioners." in "Numerical solution of partial differential equations on parallel computers, Lecture notes in computational science and engineering", *Springer*, Heidelberg, Germany, Editors: A.M. Bruaset, and A. Tveito, Aslak, Chapter 8, pp. 267-294.

Favre, H. (1935). "Etude Théorique et Expérimentale des Ondes de Translation dans les Canaux Découverts." ('Theoretical and Experimental Study of Travelling Surges in Open Channels.') *Dunod*, Paris, France (in French).

Felder, S., and Chanson, H. (2014). "Air–water Flows and Free-surface Profiles on a Non-uniform Stepped Chute." *Journal of Hydraulic Research*, IAHR, Vol. 52, No. 2, pp. 253-263 (DOI: 10.1080/00221686.2013.841780).

Felder, S., and Chanson, H. (2015). "Phase-Detection Probe Measurements in High-Velocity Free-Surface Flows including a Discussion of Key Sampling Parameters." *Experimental Thermal and Fluid Science*, Vol. 61, pp. 66-78 (DOI: 10.1016/j.expthermflusci.2014.10.009).

Henderson, F.M. (1966). "Open Channel Flow." *MacMillan Company*, New York, USA.

Hunt, J.C.R., Wray, A.A., and Moin, P. (1988). "Eddies, streams, and convergence zones in turbulent flows." *Proceedings of the Summer Program*, Center for Turbulence Research, Editors P. MOIN, W.C. REYNOLDS and J. KIM, pp. 193-208.

Khezri, N. (2014). "Modelling Turbulent Mixing and Sediment Process Beneath Tidal Bores: Physical and Numerical Investigations." *Ph.D. thesis*, The University of Queensland, School of Civil Engineering, Brisbane, Australia, 267 pages.

Leng, X., and Chanson, H. (2015). "Turbulent Advances of a Breaking Bore: Preliminary Physical Experiments." *Experimental Thermal and Fluid Science*, Vol. 62, pp. 70-77 (DOI: 10.1016/j.expthermflusci.2014.12.002).

Leng, X., and Chanson, H. (2016). "Coupling between Free-surface Fluctuations, Velocity Fluctuations and Turbulent Reynolds Stresses during the Upstream Propagation of Positive Surges, Bores and Compression Waves." *Environmental Fluid Mechanics*, Vol. 16, No. 4, pp. 695-719 & digital appendix (DOI: 10.1007/s10652-015-9438-8).

Leng, X., and Chanson, H. (2017). "Upstream Propagation of Surges and Bores: Free-Surface Observations." *Coastal Engineering Journal*, Vol. 59, No. 1, paper 1750003, 32 pages & 4 videos (DOI: 10.1142/S0578563417500036).

Leng, X., Lubin, P., and Chanson, H. (2017). "CFD Modelling of Breaking and Undular Tidal Bores with Physical Validation." *Proceedings of 37th IAHR World Congress*, IAHR & USAINS Holding Sdn. Bhd. Publ., Editors Aminuddin Ab. Ghani, Ngai Weng Chan, Junaidah Ariffin, Ahmad Khairi Abd Wahab, Sobri Harun, Amir Hashim Mohamad Kassim and Othman Karim, Kuala Lumpur, Malaysia, 13-18 August, Vol. 7, Theme 7.1, pp. 5072-5081 (ISSN 2521-7127 (USB); ISSN 2521-716X (Online)).

Leng, X., and Chanson, H. (2018). "Two-phase Flow Characteristics of a Breaking Tidal Bore Roller: Microscopic Properties." *Hydraulic Model Report No. CH109/18*, School of Civil Engineering, The University of Queensland, Brisbane, Australia.

Li, X., Arienti, M., Soteriou, M.C., and Sussman, M.M. (2010). "Towards an Efficient, High-Fidelity Methodology for Liquid Jet Atomization Computations." *Proceedings 48th AIAA Aerospace Sciences Meeting Including the New Horizons Forum and Aerospace Exposition*, 4-7 January, Orlando FL USA, Paper AIAA 2010-210, 16 pages.

Lu, H.Y., Pan, C.H., and Zeng, J. (2009). "Numerical simulation and analysis for combinational effects of two bridges on the tidal bore in the Qiantang River." *Proceedings of 5th International Conference on Asian and Pacific Coasts*, Singapore, Vol. 3, pp. 325-333.

Lubin. P., (2004). "Large Eddy Simulation of Plunging Breaking Waves." *Ph.D. Thesis*, Université Bordeaux I, France (in English).

Lubin, P., and Glockner, S. (2015). "Numerical simulations of three-dimensional plunging breaking waves: generation and evolution of aerated vortex filaments." *Journal of Fluid Mechanics*, Vol. 767, pp. 364-393 (DOI: 10.1017/jfm.2015.62).

Lubin, P., S. Vincent, S. Abadie, and J.-P. Caltagirone (2006). "Three-dimensional large eddy simulation of air entrainment under plunging breaking waves." *Coastal Engineering*, Vol. 53, No. 8, pp. 631-655.

Lubin, P., Glockner, S., and Chanson, H. (2010). "Numerical Simulation of a Weak Breaking Tidal Bore." *Mechanics Research Communications*, Vol. 37, No. 1, pp. 119-121 (DOI: 10.1016/j.mechrescom.2009.09.008).

Montes, J.S. (1998). "Hydraulics of Open Channel Flow." *ASCE Press*, New-York, USA, 697 pages.

Peregrine, D.H. (2003). "Water wave impact on walls." *Annual Review of Fluid Mechanics*, Vol. 35, pp. 23-43.

Simon, B., P. Lubin, S. Glockner, and H. Chanson (2011). "Three-dimensional numerical simulation of the hydrodynamics generated by a weak breaking tidal bore." *Proc. 34th IAHR World Congress, 33rd Hydrology and Water Resources Symposium and 10th Conference on Hydraulics in Water Engineering*. Brisbane, Australia: Eric Valentine, Colin Apelt, James Ball, Hubert Chanson, Ron Cox, Robert Ettema, George Kuczera, Martin Lambert, Bruce Melville and Jane Sargison, pp. 133-1140.

Roache, P.J. (2009). "Perspective: Validation - What does it mean?" *Journal of Fluids Engineering*, ASME, Vol. 131, March, Paper 034503, 4 pages.

Sun, S., Leng, X., and Chanson, H. (2016). "Rapid Operation of a Tainter Gate: Generation Process and Initial Upstream Surge Motion." *Environmental Fluid Mechanics*, Vol. 16, No. 1, pp. 87-100 (DOI: 10.1007/s10652-015-9414-3).

Toombes, L. (2002). "Experimental Study of Air-Water Flow Properties on Low-Gradient Stepped Cascades." *Ph.D. thesis*, Dept. of Civil Engineering, The University of Queensland, Brisbane, Australia.

Tricker, R.A.R. (1965). "Bores, Breakers, Waves and Wakes." *American Elsevier Publ. Co.*, New York, USA.

Valiani, A. (1997). "Linear and Angular Momentum Conservation in Hydraulic Jump." *Journal of Hydraulic Research*, IAHR, Vol. 35, No. 3, pp. 323-354.

Wang, H. (2014). "Turbulence and Air Entrainment in Hydraulic Jumps." *Ph.D. thesis*, School of Civil Engineering, The University of Queensland, Brisbane, Australia, 341 pages & Digital appendices (DOI: 10.14264/uql.2014.542).

Wang, H., Murzyn., and Chanson, H. (2015). "Interaction between Free-Surface, Two-Phase Flow and Total Pressure in Hydraulic Jump." *Experimental Thermal and Fluid Science*, Vol. 64, pp. 30-41 (DOI: 10.1016/j.expthermflusci.2015.02.003).

Wang, H., Leng, X., and Chanson, H. (2017). "Bores and Hydraulic Jumps. Environmental and Geophysical Applications." *Engineering and Computational Mechanics*, Proceedings of the Institution of Civil Engineers, UK, Vol. 170, No. EM1, pp. 25-42 (DOI: 10.1680/jencm.16.00025).

Wang, Z., Yang, J., and Stern, F. (2016). "High-Fidelity Simulations of Bubble, Droplet and Spray Formation in Breaking Waves." *Journal of Fluid Mechanics*, Vol. 792, pp. 307-327 (DOI: 10.1017/jfm.2016.87).

Wood, I.R. (1984). "Air Entrainment in High Speed Flows." *Proc. Intl. Symp. on Scale Effects in Modelling Hydraulic Structures*, IAHR, Esslingen, Germany, H. KOBUS editor, paper 4.1, 7 pages.

Wood, I.R. (1985). "Air Water Flows." *Proc. 21st IAHR Biennial Congress*, Melbourne, Australia, Keynote address, pp. 18-29.